


Green Synthesized Magnesium Oxide Nanoparticles Reinforce Osteogenesis Properties of Bacterial Cellulose Scaffolds for Bone Tissue Engineering Applications: An *In Vitro* Assessment

Elham Ghanbari, Ph.D.¹, Mozafar Khazaei, Ph.D.², Ahmad Mehdipour, Ph.D.¹, Ali Baradar Khoshfetrat, Ph.D.³, Behrooz Niknafs, Ph.D.^{4*} 

1. Department of Tissue Engineering, Faculty of Advanced Medical Sciences, Tabriz University of Medical Sciences, Tabriz, Iran
2. Fertility and Infertility Research Centre, Health Technology Institute, Kermanshah University of Medical Sciences, Kermanshah, Iran
3. Faculty of Chemical Engineering, Sahand University of Technology, Tabriz, Iran
4. Immunology Research Centre, Tabriz University of Medical Sciences, Tabriz, Iran

Abstract

Objective: The use of biocompatible scaffolds with appropriate characteristics to treat large bone defects has attracted significant attention. The main objective of the current study is to fabricate a 3D nanocomposite structure that contains green synthesized magnesium oxide nanoparticles (MgONPs) and bacterial cellulose (BC) nanofibres, as a bioscaffold for bone regeneration.

Materials and Methods: In this experimental study, *Camellia sinensis* extract was used as the green method to synthesize MgONPs. The synthesized hydrogels were evaluated for their porosity, morphology, degradation rate, mechanical features, cell attachment, and cytocompatibility. Osteogenic differentiation was assessed by alkaline phosphatase (ALP) activity, real-time reverse transcription-polymerase chain reaction (RT-PCR), and alizarin red staining.

Results: MgONPs significantly increased both mechanical strength ($P=0.009$) and porosity ($P=0.01$) of the BC hydrogels. Human MG-63 osteoblast proliferation significantly increased in the MgONP-BC group compared to the pure BC group ($P=0.003$). Expression rates of both the *ALP* ($P=0.001$) and osteocalcin (*OCN*) genes were significantly enhanced in cells seeded on the MgONP-incorporated BC. MG-63 cells had significantly greater calcium deposition and ALP activity ($P=0.002$) on the MgONP-BC scaffold compared to the BC at day 21.

Conclusion: The MgONP-BC scaffold can promote the osteogenic activity of osteoblast-like cells, which indicates its therapeutic potential for bone tissue regeneration.

Keywords: Bacterial Cellulose, Magnesium Oxide, Nanoparticles Osteogenesis

Citation: Ghanbari E, Khazaei M, Mehdipour A, Khoshfetrat AB, Niknafs B. Green synthesized magnesium oxide nanoparticles reinforce osteogenesis properties of bacterial cellulose scaffolds for bone tissue engineering applications: an in vitro assessment. *Cell J.* 2023; 25(7): 483-495. doi: 10.22074/CELLJ.2023.1986179.1204

This open-access article has been published under the terms of the Creative Commons Attribution Non-Commercial 3.0 (CC BY-NC 3.0).

Introduction

Bone tissue can repair itself; however, self-healing may not adequately repair the injured tissue in large bone defects (>3 cm) that occur with surgical removal and in congenital defects. Though various types of bone graft are available to restore function and improve defects (1), autograft bone remains the gold standard for defect reconstruction as it provides osteoinductive growth factors, an osteoconductive scaffold, and osteogenic cells, all of which are essential for new bone growth. Disadvantages of autografts include pain and scarring at the donor site, antigenicity, and the transmission of infectious diseases. Xenografts and allografts carry the risk of immune rejection and disease transmission upon transplantation. Synthetic bone grafts are promising substitutes for treatment

of bone defects because of the limitations associated with bone autografts, xenografts, and allografts (2).

Advantages of synthetic bone substitutes include adequate availability and lack of disease transmission. Tissue engineering techniques to generate artificial bone grafts that mimic natural bone tissue while overcoming traditional graft disadvantages have emerged (3). Bacterial cellulose (BC) has attracted considerable interest in biomedicine because of its intrinsic three-dimensionality, high chemical purity, renewable nature, lightweight nature, and high biocompatibility properties compared to other types of cellulose (4, 5). The incorporation of different bioactive materials like gold nanoparticles into the network of a BC hydrogel can improve its

physicochemical properties and stimulate osteogenic activity of the implanted scaffold (6). BC scaffolds in their natural state, however, are not bioactive materials; thus, their application in bone tissue engineering (BTE) is inevitably limited. To address this issue, scaffolds that incorporate nanoparticles such as hydroxyapatite have been proposed (7).

Magnesium oxide nanoparticles (MgONPs) are bioactive materials that can accelerate bone growth (8), yet few studies have investigated the effect of MgO in direct contact with osteogenic cells either *in vitro* or *in vivo*. One previous study reported that MgO powder implanted into the marrow cavity of rat tibia caused a 25% increase in bone thickness. Results of studies have shown an increase in alkaline phosphatase (*ALP*) gene expression of osteoblasts and proliferation when cultured on polymer/MgONP composites, which makes this family of composites more attractive for further research (9, 10).

There are a limited number of publications on green synthesized MgONP-BC as a biomaterial for bone regeneration. Thus, the current study explores the effects of MgONP-incorporated BC scaffolds on *ALP* activity, viability, cell morphology, and osteogenesis-related gene expression, of *ALP*, osteocalcin (*OCN*), and runt-related transcription factor 2 (*Runx2*).

Materials and Methods

This research was approved by the Ethics Committee of Tabriz University of Medical Sciences, Tabriz, Iran (IR.TBZMED.REC.1400.376). No human or animal subjects were used in this research.

Nanocomposite scaffold preparation

Colonies of *Acetobacter xylinum* ATCC 53582 were cultured in Hestrin & Shramm broth [H&S; 0.5% (w/v) yeast extract, 2% (w/v) glucose, 0.5% (w/v) peptone, 0.15% (w/v) citric acid, and 0.27% (w/v) Na_2HPO_4 , pH=5.0]. After the cells were cultured under static conditions at 30°C for two days, an aliquot of these cells was transferred to 50 ml H&S broth (1:10 culture-to-H&S broth ratio) and incubated at 30°C for five days. BC pellicles formed at the air/water interface during growth. The BC pellicles were rinsed with 1% NaOH distilled water and incubated at 90°C for 15 minutes to eliminate the bacteria. The BC layers were rinsed multiple times with distilled water to ensure that the NaOH was totally removed (7). Then, hydrated BCs were stored at -20°C for one day and lyophilized for 48 hours in a freeze dryer (FD10 Freeze Dryer, Tabriz, Iran). The dried BC were soaked in aqueous MgONPs solution (3% w/v) at ambient temperature under magnetic stirring for 72 hours to enable a reaction with the BC fibrils (7, 11). Afterwards, all scaffolds were sterilized by UV light exposure for two hours prior to cell culture.

Synthesis of magnesium oxide nanoparticles

Green synthesis of magnesium oxide nanoparticles using *Camellia sinensis* extracts and chemical synthesis of nanoparticles

We mixed 10 g of dried *Camellia sinensis* herb with 100 ml of double-distilled deionized water; the mixture was boiled at 70°C for 30 minutes with continuous stirring. The prepared solution was filtered through Whatman's No. 1 paper. The obtained extract was mixed with magnesium chloride hexahydrate ($\text{MgCl}_2 \cdot 6\text{H}_2\text{O}$) in a 90:10 v/w ratio and continuously stirred for 4 hours at 70°C. Suspensions were centrifuged (10 000 rpm/10 minutes). Finally, the MgONP pellets were collected, washed with deionized water, and dried at 40°C for two hours. The prepared powders were then calcined for three hours at 500°C. Subsequently, the MgONPs were subjected to several assays in order to confirm nanoparticle formation (8). The chemical synthesized MgONPs were prepared according to a previously published technique (10).

Characterisation of magnesium oxide nanoparticles

UV-visible spectroscopy analysis

MgO nanopowders were resuspended to produce a dilute suspension, and their synthesis was examined by UV-visible (UV-vis) spectroscopy (Shimadzu, Japan) at the range of 200-800 nm.

Dynamic light scattering and zeta potential measurements

The stability and size of green synthesized MgONPs were evaluated by zeta potential (ZP) and a dynamic light scattering (DLS) analyser (Malvern Zetasizer nano-ZS90, UK), respectively.

Antibacterial effects of magnesium oxide nanoparticles

The antibacterial effects of the MgONPs against *Staphylococcus aureus* (*S. aureus*), methicillin-resistant *S. aureus*, *Pseudomonas aeruginosa* (*P. aeruginosa*), and methicillin-resistant *P. aeruginosa* were assessed by disk diffusion. *S. aureus*, methicillin-resistant *S. aureus*, *P. aeruginosa*, and methicillin-resistant *P. aeruginosa* were prepared with a suspension equivalent to 1.5×10^8 CFU/mL McFarland and cultured with a sterile swab on the surfaces of Müller-Hinton agar plates. Sterile paper discs (5 mm) were impregnated with different concentrations of MgO-NP suspension (1 and 5%) and placed on the surface of the agar medium by using sterile forceps. The plates were incubated at 37°C for 24 hours, after which the clear halo of stunting was measured. The findings were described according to the diameter of the clear zone (inhibition zone) around each disk (12, 13). Tests were carried out in triplicate.

Characterisation of scaffolds and magnesium oxide nanoparticles

Fourier transform infrared spectroscopy

Fourier transform infrared spectroscopy (FTIR) spectroscopy (Nicolet 8700 spectrometer; Thermo Fisher Scientific, Waltham, MA, USA) was used to determine the functional group of the dried MgONPs and scaffolds (14). Spectra data were recorded over a wavenumber range of 400-4000/cm.

Morphological analysis of scaffolds and magnesium oxide nanoparticles

The morphology and size of the MgONPs were determined by field emission scanning electron microscopy (SEM, Carl Zeiss, Germany). Specimens (scaffolds and MgONPs) were covered with gold and observed at an accelerating voltage of 15 kV. The composition of MgONPs and *Camellia sinensis* leaf extract was analysed by SEM-energy-dispersive X-ray (SEM-EDX) spectroscopy (14).

Mechanical characterisation of scaffolds

The mechanical strength of the scaffolds was evaluated using a Universal Testing Machine (Instron 4505) equipped with a 1 kN load cell at room temperature. The tested specimens were cut into "round disk" shapes with dimensions of 5 mm height and 1 cm diameter. The cross-head speed was adjusted to 2 mm/minute, and the load was set to a 70% reduction in specimen height. The stress-strain curve was plotted, and the slope of the first linear segment of the curve (n=4) was used to determine Young's modulus.

Porosity study

The porosity of various scaffolds was measured using the liquid displacement procedure. Briefly, the scaffold (1 cm diameter and 5 mm thickness) was soaked for 30 minutes in volume V1 of ethanol. The total volume of the ethanol and scaffold after complete immersion was V2, and the residual volume after the ethanol-impregnated scaffold was removed was V3. The following formula was used to calculate the porosity of scaffolds:

$$P (\%) = (V1 - V3) / (V2 - V3)$$

The test was performed four times to obtain the average porosity value (15).

Degradation rate and Mg²⁺ release of scaffolds

The scaffold degradation rate was determined by immersing the specimens (10-mm diameter and 2-mm thickness) in a phosphate-buffered saline (PBS) solution of pH=7.4 at 37°C for 21 days. After incubation at various time periods (7, 13, and 21 days), the scaffolds were removed from the degradation medium, rinsed with distilled water, and dried in a

vacuum oven.

$$\text{Degradation rate} = (WO - WT) / (WO) \times 100$$

W0 and WT represent, respectively, the initial weight of the scaffolds before and after immersion in PBS up to day T (8). The Mg²⁺ release assay was carried out using the protocol of Suryavanshi et al. (10).

In vitro swelling evaluation

Swelling potential was evaluated by soaking the scaffolds in PBS buffer solution with pH=7.4 for 2, 6, 24, 48, and 72 hours (n=4). The percentage of increase in water uptake was calculated using the following equation:

$$\text{Swelling ratio (\%)} = (Wt - W0) / W0 \times 100$$

Where: Wt is the weight of wet scaffolds at time t and W0 is the weight of dry scaffolds (15).

In vitro biological evaluation

Viability/cytotoxicity assay

The MTT assay was used to assess viability of cells seeded (density: 3×10³ cells) on the scaffolds on days 7, 14, and 21. Briefly, 150 μL of the 0.5 mg/mL MTT solution was added to the scaffolds/cells, which were then incubated for three hours at 37°C and 5% CO₂, and then removed from the solution. After incubation, 50 μL DMSO was added to dissolve the formazan crystals, and the plate was read by an ELISA microplate reader at 570 nm (Biorad, Hercules, CA, USA).

Percentage of cell viability was calculated using the following equation:

$$\text{Percentage cell viability} = \text{OD Sample} / \text{OD Control} \times 100$$

OD_t = The OD of cells/scaffold; OD_c = the OD of control cell (15).

Cell seeding on scaffolds and culture conditions

Human MG-63 osteoblast-like cells were cultured in Dulbecco's Modified Eagle Medium (DMEM) low glucose supplemented with 1% (v/v) penicillin/streptomycin solution, 50 mg/L ascorbic acid, 10 mmol/L β-glycerophosphate, 10 nmol/L dexamethasone, and 10% (v/v) foetal bovine serum, and incubated at 37°C with 5% CO₂ and 95% relative humidity. During the 21-day study period, the medium was renewed every three days. When the MG-63 cells reached 70-80% confluency, they were detached using a 0.25% trypsin-EDTA solution (Gibco). Thereafter, 50 μl of cell suspension that contained 2×10⁵ cells was slowly dropped onto the surface of the UV-sterilized scaffolds (15).

Cell distribution

We applied 4',6-diamidino-2-phenylindole (DAPI)

staining to assay MG-63 cell proliferation on the scaffolds. After washing with PBS, the samples were fixed with 3.7% paraformaldehyde for three hours, stained with DAPI, and observed under a fluorescence microscope (Nikon Eclipse Ti2, Japan).

Measurement of oxidative stress in scaffolds

The total antioxidant capacity (TAC) and nitric oxide (NO) level of the collected supernatants of the cells seeded on the scaffolds were determined using ferric reducing power (FRAP) and the NO assay, respectively (17, 18).

Osteogenic measurements

Alkaline phosphatase activity determination

The ALP activity of the cells cultured on different scaffolds was determined after incubation for 7, 14, and 21 days by an ALP assay kit (Pars Azmoon, Iran) according to the manufacturer's instructions. Finally, ALP activities were normalized versus the total protein content (19).

Alizarin red staining for mineralisation assay

The mineralisation of MG63 cells after incubation for 21 days was quantitatively measured using the alizarin red staining assay (19). The alizarin red staining concentration was evaluated by absorbance measurement using a spectrophotometer (Pharmacia, Novaspec II, Biochrom, England) at a wavelength of 405 nm.

Bone-associated gene expression assay

The real-time reverse transcription-polymerase chain reaction (RT-PCR) method was performed to evaluate the expression levels of *ALP*, *OCN*, and runt-related transcription factor 2 (*Runx2*) genes after 21 days of cell culture. Briefly, total RNA was extracted from the cell-seeded scaffolds by TRIzol/chloroform based on the manufacturer's protocol (Life Biolab, Heidelberg, Germany). Then, cDNA was synthesized from total RNA by using an AddScript cDNA synthesis kit (AddBio, South Korea) and oligo dT20 and random hexamers. RT-PCR was performed by Ampliqon SYBR Green Master Mix (RealQ Plus 2x Master Mix, Ampliqon, Denmark) and then carried out in a Step One Plus™ system (Applied Biosystems, USA). The expression levels of the *Runx2*, *OCN*, and *ALP* genes were calculated by RT-PCR and normalized using glyceraldehyde 3-phosphate dehydrogenase (*GAPDH*) as the housekeeping gene. The relative changes in intended gene expression were assessed using the $2^{-\Delta\Delta CT}$ method. The designed primers used in this experimental study are listed below:

ALP- Human-

F: 5'-GCTGGGAAATCTGTGGGC-3'

R: 5'-CCATGATCACGTCAATGTCCCT-3'

Runx2- Human-

F: 5'-TCATGGCGGGTAACGATGA-3'

R: 5'-GGGAGGATTTGTGAAGACGG-3'

OCN- Human

F: 5'-CAGCCACCGAGACACCATGA-3'

R: 5'-CTTGGACACAAAGGCTGCAC-3'

GAPDH- Human

F: 5'-AAGGTGAAGGTCGGAGTCAAC-3'

R: 5'-GGGGTCATTGATGGCAACAA-3'

Statistical analysis

All quantitative data are reported as mean \pm standard deviation (n=4). Statistical significance was determined as a $P < 0.05$ using one-way analysis of variance (ANOVA) and Tukey's post hoc test in GraphPad Prism, version 8.4.3 (San Diego, CA, USA).

Results

Characterisation of magnesium oxide nanoparticles and scaffolds

UV-visible spectroscopy assay

Figure 1A and B show UV-vis spectroscopy images of the synthesized MgONPs. The MgONPs prepared by chemical synthesis had a maximum peak of 325 nm (Fig.1A), whereas MgONPs prepared by green synthesis showed a maximum peak of 285 nm (Fig.1B).

Dynamic light scattering and zeta potential of magnesium oxide nanoparticles

We conducted DLS analysis to determine the dispersion and size of MgONPs in the colloidal solution through the reaction of light beams with biosynthesized MgONPs. The green synthesized MgONPs were observed at 56.03 to 88.33 nm with a polydispersed index value of 0.484. The average size of the MgONPs was 72.18 nm (Fig.1C).

The ZP, a key indicator of the stability of the colloidal dispersions and surface charge of nanoparticles, was -19.1 ± 5.86 mV in the biosynthesized MgONP sample, which indicated that the colloidal solution was stable (Fig.1D) and that the MgONPs had a negative surface charge based on their area.

Morphology observation by scanning electron microscopy

Figure 1E shows the morphology and size of biosynthesized MgONPs as observed by SEM. The MgONPs had compact agglomerates. These images also showed that the biosynthesized MgONPs had spherical morphologies with high aggregation, which confirmed polydispersity in the DLS analysis (Fig.1E). EDX analysis of the extract (Fig.1F) and green synthetic MgONPs (Fig.1G) showed the purity of the nanoparticles and confirmed formation of these nanoparticles with strong signals in the O and Mg regions. Quantitative analysis results indicated that the weight percentages of O and Mg ions in the sample were 54.1 and 20.6%, respectively, while the atomic ratio was 50.3 and 17.1%, respectively (Fig.1F).

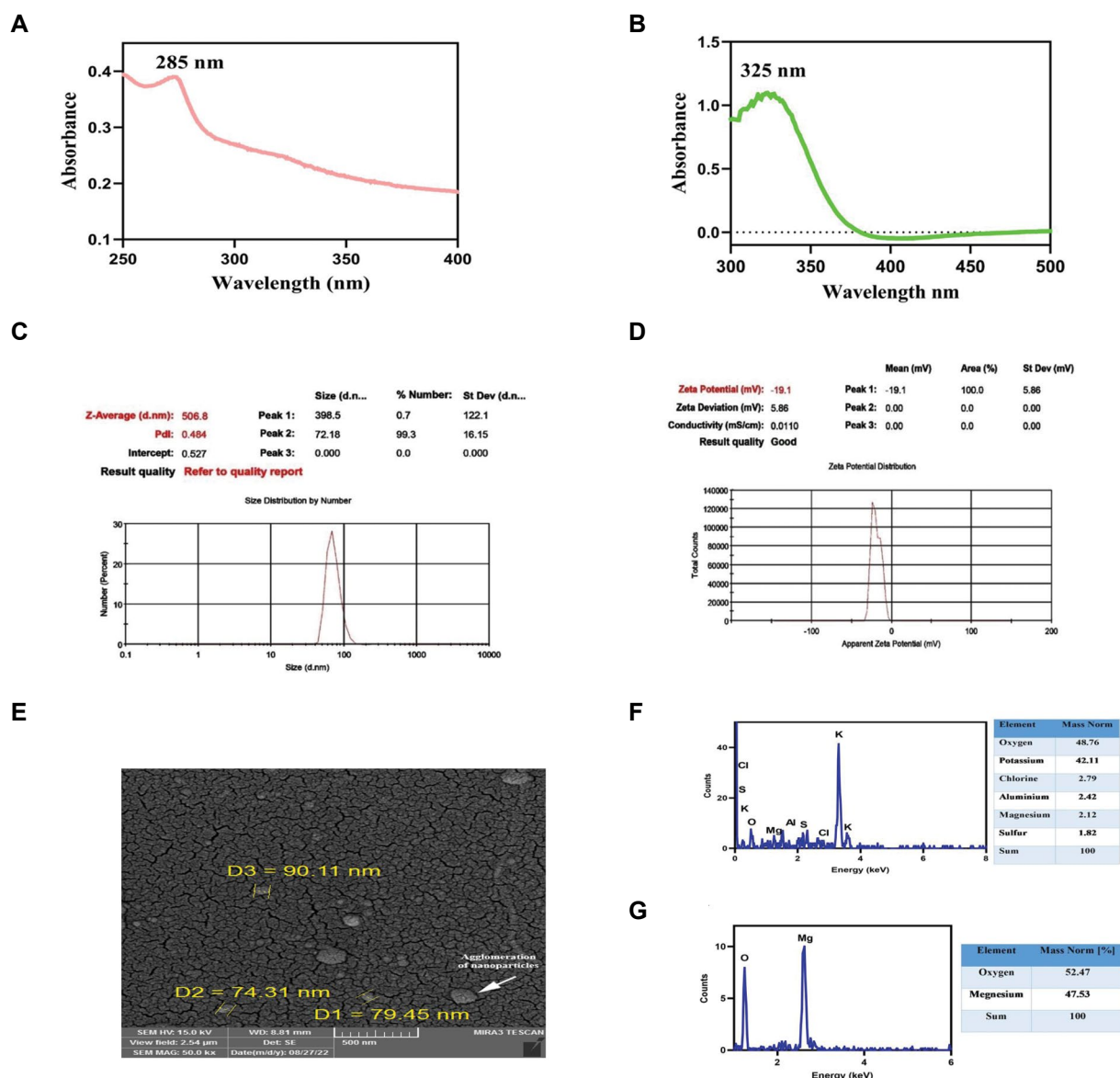


Fig.1: Analysis of UV-vis, DLS, ZP, SEM and EDX spectrum tests for MgONPs in different groups. **A.** UV-vis analysis of chemical synthesized MgONPs and **B.** MgONPs synthesized by *Camellia sinensis*. **C.** DLS analysis of MgONPs synthesized using *Camellia sinensis* extract. **D.** ZP analysis of biosynthesized MgONPs. **E.** SEM analysis of MgONPs synthesized using *Camellia sinensis*. **F.** EDX spectrum analysis shows major peak of extract and **G.** MgONPs synthesized by *Camellia sinensis* extract, which corresponds to the MgONPs. UV-vis; UV-visible, DLS; Dynamic light scattering, ZP; Zeta potential, SEM; Scanning electron microscopy, EDX; Energy-dispersive X-ray, and MgONPs; Magnesium oxide nanoparticles.

Fourier-transform infrared spectroscopy characterisation

FTIR spectra of the MgO nano-powder and green synthesized MgONPs are presented in Figure 2A. The stretching bond at 470.63 cm^{-1} clearly confirmed the formation of green synthesized MgONPs. The existence of several bioactive metabolites such as anthocyanins, tannins, and flavonoids was attributed to the strong band observed near 3441.01 cm^{-1} for the O–H bond vibration of the hydroxy group. The stretching vibration of C=C was responsible for the band at $1633\text{--}1651\text{ cm}^{-1}$, whereas the stretching vibration of C=C and the bending of the N–H bond were responsible for the band at $1462\text{--}1539\text{ cm}^{-1}$. The stretching vibration of the C–O bond was attributed to the band at 1089.78 cm^{-1} (Fig.2A).

Antibacterial activity of magnesium oxide nanoparticles

The data did not show any significant difference related to antibacterial activity of the green and chemically synthesized MgONPs (1 and 5% w/v) for *S. aureus*, *P. aeruginosa*, and methicillin-resistant *P. aeruginosa* ($P=0.08$) (Fig.2B, D-G). The antibacterial activity of green synthesized MgONPs at the 1% and 5% w/v suspensions significantly inhibited the growth of methicillin-resistant *S. aureus* compared to the *Camellia sinensis* extract ($P=0.003$, Fig.2F). The green synthesized MgONPs at the 5% concentration (Fig.2C, F) had the largest inhibition zones ($P=0.001$, Fig.2F).

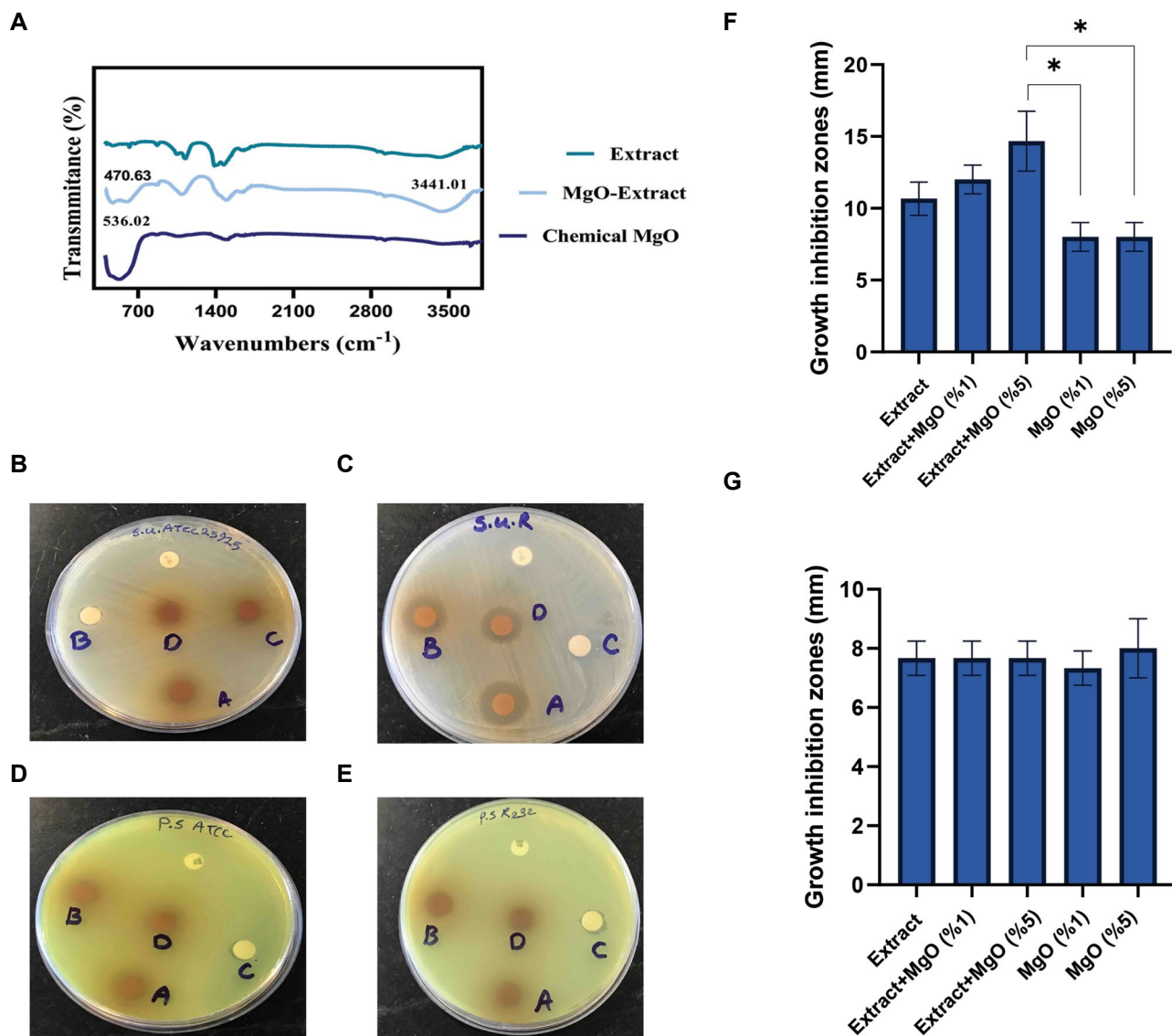


Fig.2: Fourier transform infrared spectroscopy (FTIR) study and antibacterial effects of magnesium oxide nanoparticles (MgONPs). **A.** FTIR spectra of green and chemically synthesized MgONPs. Results of disc diffusion tests to determine the antibacterial effects of green and chemically synthesized MgONPs (1 and 5%). **B.** *Staphylococcus aureus* (*S. aureus*), **C.** methicillin-resistant *S. aureus*, **D.** *Pseudomonas aeruginosa* (*P. aeruginosa*), **E.** Methicillin-resistant *P. aeruginosa*. **F.** Growth inhibition zone of *S. aureus* and methicillin-resistant *S. aureus*, and **G.** growth inhibition zone of *P. aeruginosa* and methicillin-resistant *P. aeruginosa*. One-way analysis of variance (ANOVA) test results for antibacterial activity of green and chemically synthesized MgONPs in the different groups. *; $P < 0.05$ growth inhibition zone decreased in green synthesized MgONPs (1, 5%) groups in comparison to the chemical synthesized MgONPs group.

Scanning electron microscopy and Fourier-transform infrared spectroscopy assay of the scaffolds

SEM images showed that a large volume of the BC scaffolds were occupied by pore interconnectivity and interwoven nanofibres (Fig.3A). Examination of the scaffolds demonstrated that MgONP-BC had a highly porous microstructure compared to the pure BC membrane (Fig.3B).

The absorption peak of the BC in FTIR was $1317-1161\text{ cm}^{-1}$: CO stretching, 1651.7 cm^{-1} : CH_2 symmetric stretching, 2895.15 cm^{-1} : asymmetric CH_2 stretching, and 3361.9 cm^{-1} : OH stretching. The major characteristic peaks of BC (3338.5 cm^{-1} to H-O, 1561.05 cm^{-1} to C-H, and 1073.14 cm^{-1} to C-O) and MgONP (590.63 cm^{-1}) were

shown in the FTIR spectra of the MgONP-BC groups. The coexistence of characteristic peaks of MgONP and BC in the spectra of the MgONP-BC hydrogels confirmed successful incorporation of MgONP into the BC network (Fig.3C).

Porosity, degradation rate, cumulative Mg^{2+} release and swelling ratio measurement of the scaffolds

Porosity investigations revealed that the scaffolds are highly porous (Fig.3D). The MgONPs-BC had a higher porosity ($89.2 \pm 4.85\%$) than pure BC ($62.9 \pm 3.49\%$). The results showed no significant difference in swelling ratio between the MgONP-BC group and the BC groups ($P > 0.05$) at 2, 6, 24, 48, and 72 hours. The swelling ratio was 75% for the BC groups and 78% for MgONP-BC after

24 hours, which increased to 79 and 88%, respectively, after 72 hours ($P=0.01$, Fig.3E).

Figure 3F shows the scaffold degradation rates in PBS (both pH=7.4) after incubation on days 1, 7, 14, and 21. There was no significant difference observed between pure BC and MgONPs-BC on days 7, 14, and 21 ($P=0.07$). The release curves of Mg^{+2} from the BC and MgONP-BC scaffolds are shown in Figure 3G. In the first week, the MgONP-BC scaffolds exhibited a relative burst release; by day 14, the composite membranes released 70-80% of the nanoparticles in a sustained manner. These findings

revealed that the MgONP-BC scaffolds continuously released nanoparticles into the external medium.

Viability/cytotoxicity assay of the scaffolds

The MTT assay was used to determine cell viability on the scaffolds (Fig.3H). Both the MgONP-BC and BC scaffolds had a positive effect on cell viability on days 7, 14, and 21. A comparison of those scaffolds showed that cell viability was significantly higher in the MgONP-BC scaffold compared to pure BC after 21 days of cell culture ($P=0.003$).

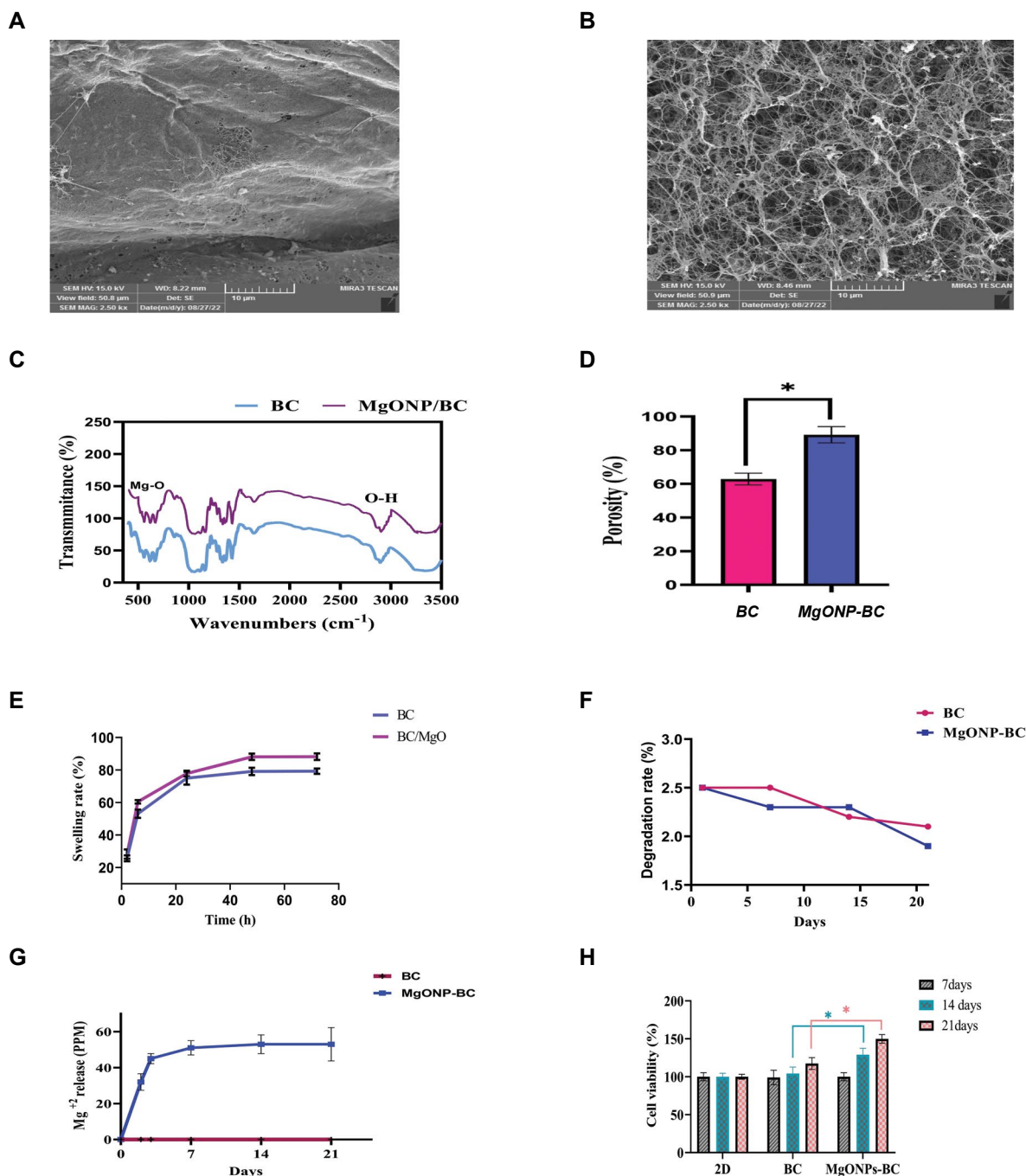


Fig.3: The analysis of SEM, porosity, swelling, degradation rate, Mg^{+2} release, and cytotoxic effects of scaffolds in the different groups. **A.** SEM image of BC and **B.** MgONP-BC scaffolds (scale bar: 10 μm). **C.** Fourier transform infrared spectroscopy (FTIR) spectra of scaffolds. ANOVA results for **D.** Porosity, **E.** Swelling, **F.** Degradation rate, **G.** Mg^{+2} release, and **H.** Cytotoxic effects of scaffolds in the different groups. *; $P \leq 0.05$ for porosity, swelling and cytotoxic effects of scaffolds increased in the MgONPs-BC groups in comparison to the BC group. SEM; Scanning electron microscopy, BC; Bacterial cellulose, MgONP; Magnesium oxide nanoparticle, and ANOVA; One-way analysis of variance.

Mechanical properties of the scaffolds

Both mechanical strength and Young's modulus were higher for MgONPs-BC scaffolds compared to the pure BC scaffold ($P=0.009$). Nonetheless, there were considerable differences in Young's moduli among all groups (Table 1). The initial linear slope of stress-strain curves was used to determine the stiffness of the scaffolds, and was calculated as Young's modulus. Young's modulus was 146.36 ± 4.24 MPa for BC and 191.19 ± 15.10 MPa for MgONP-BC.

Table 1: Young's modulus and compressive strength of various scaffolds

Sample	Young's modulus (MPa)	Compressive strength (MPa)
Pure BC	146.36 ± 4.24	36.19 ± 3.18
MgONPs-BC	$191.19 \pm 15.10^*$	$53.09 \pm 5.02^{##}$

One-way analysis of variance (ANOVA) test results for Young's modulus and compressive strength in the research groups. *, $P \leq 0.01$ Young's modulus increased in the magnesium oxide nanoparticle-bacterial cellulose (MgONPs-BC) groups in comparison to the BC group and ##; $P \leq 0.01$ increased compressive strength in the MgONPs-BC group compared to the BC group.

Assessment of total antioxidant capacity and nitric oxide levels

Figure 4A shows the TAC levels. After 14 days, the

MgONP-BC scaffolds had higher TAC than the BC scaffolds ($P=0.004$). After 21 days of incubation, however, TAC levels in the MgONP-BC scaffolds did not show any significant difference compared with pure BC scaffolds ($P=0.05$). According to Figure 4B, there was a significant difference in NO level for the MgONP-BC scaffolds. NO levels significantly decreased ($P=0.001$) after 21 days in the MgONP-BC scaffolds compared with the pure BC scaffolds.

Cell distribution

DAPI staining was used to evaluate cell proliferation on the scaffolds. After seven days of culture, the number of cells in the biosynthesized MgONPs-BC scaffold (Fig.5A) increased in comparison with the pure BC scaffold (Fig.5B). Overall, MgONPs appeared to improve cell proliferation on the BC scaffolds; therefore, they were used in this study. MG-63 cells were cultured on a plate with the same cell culture conditions on the scaffold and considered to be a two-dimensional (2D) group (Fig.5C).

Osteogenic measurements

Alizarin red staining for mineralisation

The green synthesized MgONP significantly enhanced mineralisation levels of cells on BC scaffolds at 21 days of incubation ($P=0.004$). These findings showed that the presence of MgONPs in the BC scaffolds could accelerate MG-63 cell mineralisation activity (Fig.5D).

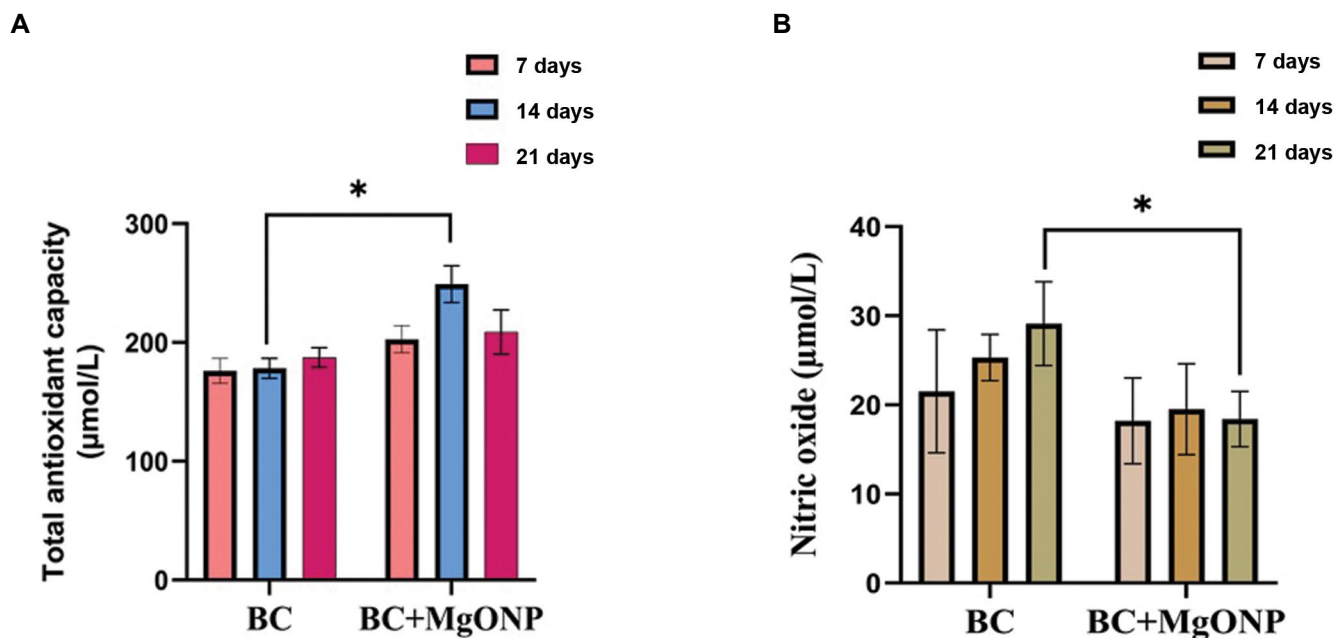


Fig.4: TAC and NO of cell-seed scaffolds. ANOVA results for TAC and NO in BC-based scaffolds. **A.** TAC increased in the MgONP-BC groups in comparison to the BC group ($*P \leq 0.05$). **B.** NO decreased in the MgONP-BC groups in comparison to the BC group ($P \leq 0.05$). TAC; Total antioxidant capacity, NO; Nitric oxide, ANOVA; One-way analysis of variance, BC; Bacterial cellulose, and MgONP; Magnesium oxide nanoparticle.

Osteogenesis-related gene expression

The MgONP-incorporated BC scaffolds exhibited increased *ALP* ($P=0.001$) and *OCN* ($P=0.004$) expressions compared with pure BC scaffolds at 21 days. No significant difference in human *Runx2* expression was observed between the MgONP-BC and pure BC scaffolds (Fig.5E).

Measurement of alkaline phosphatase activity

The MG-63 cells on BC showed lower ALP activity compared to the MgONP-BC scaffolds after 14 ($P=0.005$) and 21 ($P=0.002$) days of cell culture (Fig.5F). ALP activity levels did not show any significant change for cells on the BC and MgONP-BC scaffolds at seven days.

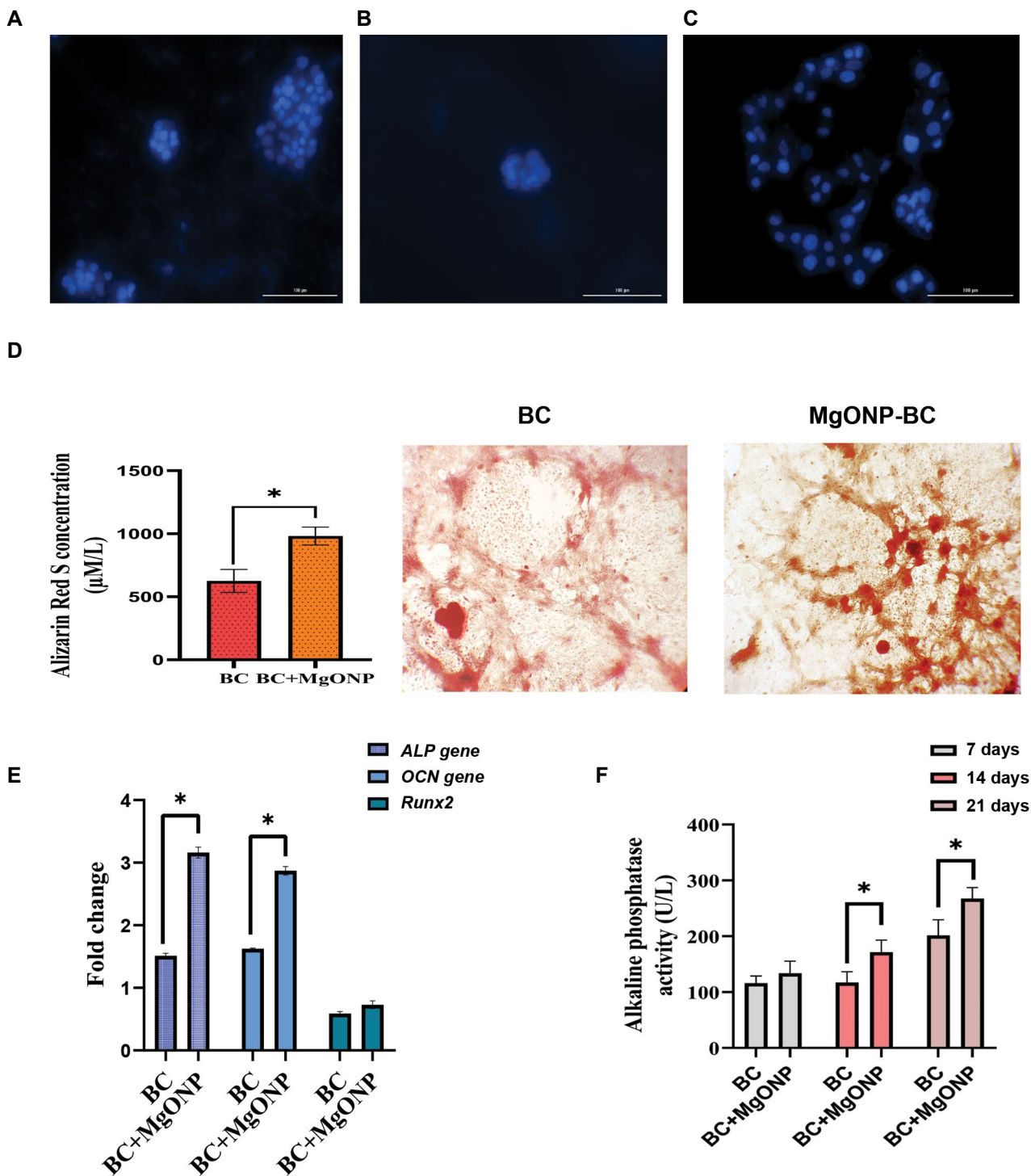


Fig.5: The analysis of 4',6-diamidino-2-phenylindole (DAPI) staining, alizarin red S concentration and gene expressions of *ALP*, *OCN*, and *Runx2* in the different groups. **A.** DAPI staining of MG-63 cells on magnesium oxide nanoparticle-bacterial cellulose (MgONP-BC), **B.** BC scaffolds, and **C.** A well plate at seven days after cell seeding (scale bar: 100 μm). **D.** One-way analysis of variance (ANOVA) test results for alizarin red S staining concentration in the different groups. *; $P \leq 0.05$ Alizarin red S staining increased in the MgONPs-BC group in comparison to the BC group (scale bar: 100 μm). **E.** ANOVA results for gene expressions of *ALP*, *OCN*, and *Runx2* in the different groups. *; $P \leq 0.05$ *ALP*, *OCN*, and *Runx2* expressions increased in the MgONPs-BC group in comparison to the BC group. **F.** *ALP* activity in cells cultured on BC and MgONP-BC scaffolds. *; $P \leq 0.05$ *ALP* activity increased in the MgONPs-BC groups in comparison to the BC group.

Discussion

Green synthesized MgONPs incorporated into BC scaffolds improved their physicochemical properties. In the current study, we proved that these MgONP-incorporated BC scaffolds increased porosity, compressive strength, cell proliferation, and mineralisation. To the best of our knowledge, this study was the first to report that MgONP-BC scaffolds could promote the osteogenic activity of MG-63 cells. UV-spectrophotometry analysis indicated a maximum absorbance peak at 322 nm, which showed the formation of small-sized green synthesized MgONPs (20). The results of this study supported those of previous studies (20), although there was a sharp absorbance peak of green synthesized MgONPs at 285 nm.

The present study revealed that the green synthesized MgONP of *Camellia sinensis* significantly inhibited bacterial growth of methicillin-resistant *S. aureus* in a dose-dependent manner. In line with this data, Ravoor et al. (21) reported that MgONPs inhibited the growth of methicillin-resistant *S. aureus*. In the current study, chemical synthesized MgONPs exhibited no antibacterial effects against *S. aureus*, methicillin-resistant *S. aureus*, methicillin-resistant *P. aeruginosa*, or *P. aeruginosa*. In the case of methicillin-resistant *S. aureus*, the highest antibacterial activity was observed at 5% w/v green synthesized MgONP. Notably, the 1% w/v and 5% w/v concentrations of green synthesized MgONP had no antibacterial activity against *S. aureus*, *P. aeruginosa*, or methicillin-resistant *P. aeruginosa*. Because *Camellia sinensis* extract had an antibacterial effect on methicillin-resistant *S. aureus*, we hypothesized that the antibacterial effect of green synthesized MgONP nanoparticles could be related to the biomolecules of the *Camellia sinensis* extract that attached to the nanoparticle surfaces.

SEM images in the current study indicated a mean diameter of 74 nm and a spherical shape for green synthesized MgONPs. DLS analysis also confirmed the ~72 nm diameter size distribution. We observed a ZP of approximately -19.1 mV, which indicated good stability of the synthesized nanoparticles.

The small size (<100 nm) of MgO offers valuable advantages for bone regeneration. First, it effectively promotes osteoblast adhesion and osteogenic activity of the nanocomposite scaffolds. Second, it stimulates the angiogenic response and reduces inflammation (22, 23). Our RT-PCR evaluation showed that MgONPs-loaded BC scaffolds had greater expression of the osteogenesis-specific marker genes *ALP* and *OCN* compared to the BC scaffolds.

ALP activity levels are important for bone mineralisation and are measured as an osteogenic marker. Based on the data, ALP levels exhibited no significant difference for the cells seeded on the scaffolds at seven days. In contrast, increased ALP

activity was seen in cells seeded on MgONP-BC scaffolds on days 14 to 21 compared to day 7. Other study results have shown that higher ALP activity is integral for ECM regeneration before mineralisation in the presence of osteoblasts (24).

The EDX result of MgONPs synthesized from the aqueous extract of *Pterocarpus marsupium* revealed two peaks for O and Mg ions with weight percentages of 69.3 and 30.6%, respectively (25). The FTIR spectrum of green synthesized MgO nanoparticles showed sharp peaks at 653.51-825.42 cm^{-1} , which corresponded to the Mg-O-Mg groups as well as at 3447.11 cm^{-1} that was attributed to the O-H bending of the hydroxy group, and was related to the presence of several bioactive metabolites (anthocyanins, tannins, and flavonoids). An absorption peak found at 1590.22 cm^{-1} corresponded to the carbonyl group of flavonoids (26). Similarly, EDX analysis of this study revealed that the green synthesized MgONPs were extremely pure, and contained both Mg and O ions.

In line with previous studies, the current study showed that the peak intensity of O-H in the FTIR spectrum of the green synthesized MgO nanoparticles increased, and the existence of broad peaks of MgO and *Camellia sinensis* extract in the FTIR spectra of green synthesized MgONPs indicated successful synthesis of the MgONPs of the plant extract; this was consistent with the EDX data.

In the present study, SEM imaging revealed high porosity in the MgONP-BC scaffolds compared to BC scaffolds. BC contains many free hydroxyl groups that react with water molecules, and this causes a reduction in pore size and porosity (27). The interaction of water molecules with the free hydrophilic functional groups of the scaffolds reduces the pores (28). Our porosity results were similar to those of Khan et al. (29), who reported that the enhancement of pore size and porosity in BC-based scaffolds incorporated with nanoparticles was related to an increase in the amount of retained water, which was most likely predominantly unbound water. Unbound water is defined as water that freezes and cause pores.

The results of other studies have shown that the magnetic nanoparticles loaded in the scaffolds acted as a backbone and improved the mechanical strength and high porosity in the nanocomposite scaffolds (30). The presence of graphene oxide (GO) nanoparticles increased the porosity and interparticle space of composite scaffolds by increasing their ability to retain water. Despite increased porosity, GO increased the mechanical properties of the scaffold because of the interactions between the fillers and the polymer matrix and improved cell attachment and proliferation (31). Chitosan-collagen scaffolds incorporated with zinc oxide nanoparticles showed higher porosity than chitosan-collagen scaffolds (32). We hypothesized that the increased water absorption in scaffolds that

contain MgONP and the interaction of nanoparticles with the free hydroxyl group of the BC scaffolds could increase the number of unbound water molecules in the scaffolds. After freezing and the freeze-drying process, larger pores form in these scaffolds.

MgONP-incorporated sodium alginate can increase mechanical strength. The results of mechanical property evaluations showed that Young's modulus of the MgONPs (4 wt%)-sodium alginate scaffolds enhanced about 44% compared with sodium alginate scaffolds. Nasri-Nasrabadi et al. (9) reported that the increase in Young's modulus at 4% MgONP could be attributed to the mobility limitations of the polymer chain and the formation of strong intra-molecular hydrogen bonds between the hydroxyl groups of the scaffold and nanoparticles. The current results showed that MgONP (3%)-BC had good porosity and mechanical strength. We hypothesized that the hydrogen/covalent bonding that occurred between the OH groups of the BC scaffolds and MgONPs enhanced the toughness and reduced the chains' mobility, and enhanced the mechanical strength of the MgONPs-BC. Numata et al. (27) demonstrated that a slow-release system that combined a BC hydrogel and nanoparticles could be effectively used in the biomedical field. In the current study, MgONPs were released in a burst from the nanofibres within 14 days with about 70-80% release for MgONP-BC.

SEM images of the BC scaffolds in the current study showed a smooth and uniform surface. After incorporation of MgONPs into the BC scaffold, the nanocomposite surface exhibited highly porous structures. Therefore, the current findings supported the results where, in the absence of silver nanoparticles, BC scaffolds formed dense structures with irregularly shaped and highly interconnected pores (33). In the present study, SEM analysis of the MgONPs-BC scaffolds showed spherical particles entrapped between the BC nanofibrils. Aggregates of nanoparticles were also observed on the nanofibres.

It is crucial to evaluate the liquid uptake ability of scaffolds when they are considered for use in tissue engineering. Improvement in the swelling ratio of scaffolds is a prerequisite for waste diffusion, facilitated nutrients and an enhanced cell attachment, and cellular interactions which enhance tissue regeneration. Although an enhancement in the swelling capacity of the scaffold seems to be significant, continuous swelling leads to a decrease in the compressive strength of the scaffold and its disintegration (34). In the current study, the swelling ability for BC and MgONP-BC scaffolds was found to be incremental at 2, 6, 24, 48, and 72 hours and this showed their ability to absorb fluids. Therefore, the presence of MgONPs did not affect the ability of the scaffolds to absorb liquids.

FTIR analysis indicated BC had typical peaks of

3361.9 cm^{-1} (O-H stretching) and 2895.15 cm^{-1} (C-H stretching), and MgONP-incorporated BC had peaks of 480.5 cm^{-1} . In the FTIR spectra of alginate/polymer (vinyl alcohol) scaffolds, the Mg-O stretching vibrational band at 540 cm^{-1} could not be isolated because those peaks overlapped significantly with the intense peaks of the scaffold (35). According to our results, a wavelength of 400-650 cm^{-1} can be used to determine the presence of MgONPs in the BC scaffold. Therefore, this study showed that MgONPs were successfully incorporated in the BC scaffold.

Previous studies have reported that green synthesized MgONPs have an antioxidant effect (36) and can stimulate some bone regeneration mechanisms (37). The differentiation of pre-osteoclasts into osteoclasts is activated by oxidative stress and enhances bone resorption. Antioxidant compounds promote osteoblast growth and bone production while inhibiting the differentiation and activity of osteoclasts. High levels of ROS have opposing effects; they inhibit osteoblast differentiation and decrease mineralisation and osteogenesis activity (38).

NO has dose-dependent effects on osteoclast and osteoblast activity. Therefore, the balance of NO levels can be important to the appropriate regeneration of critical-size bone defects. Low NO levels lead to increased osteoblast proliferation and bone formation, while high NO levels stimulate osteoblast apoptosis (39). These obtained results agree with the current results, in which NO levels were reduced in MgONP-BC compared to BC scaffolds, while TAC levels were significantly higher for MgONP-BC scaffolds than for pure BC scaffolds.

DAPI-stained images on day 7 of the study revealed an enhanced number of cells in the MgONP-BC compared to the other groups. MTT analysis also exposed an increased cell survival rate in cells on the MgONP-BC scaffolds.

The current results introduce MgONP-BC nanocomposite as an advisable high-performance scaffold for BTE applications. Some limitations in areas of this study that need further attention include the lack of investigation into the osteogenic effects of MgONP-BC *in vivo*. This evaluation can provide valuable data about the behaviour of scaffolds in healing of bone defects. These MgONP-BC scaffolds elevate the osteogenic differentiation of MG-63 cells and display good cytocompatibility, which indicates their feasibility as a biomaterial for bone regeneration.

Conclusion

Green synthesized MgONPs showed antioxidant and antibacterial effects. After loading, the BC scaffold exhibited good biological characteristics for cell attachment and proliferation. MgONP-BC scaffolds could overcome the limitations of cell adhesion and

mineralisation during the bone regeneration process in vitro. The MgONP-BC hydrogel could be an efficient system for bone regeneration, and MgONPs can be suggested as a bioactive factor in bone repair; therefore, in vivo experiments on the use of these additive materials are recommended.

Acknowledgements

Funding for this study was provided by the Immunology Research Centre, Tabriz University of Medical Sciences, Tabriz, Iran. This study is a part of a Ph.D. thesis registered in Tabriz University of Medical Sciences with the number 66827. The authors have no conflicts of interest.

Authors' Contributions

E.Gh., B.N., M.Kh., A.M., A.B.K.; Participated in study design, Methodology, Data collection, Analysis, and Interpretation. E.Gh., M.Kh., A.B.K.; Wrote, Reviewed, and Edited the manuscript. All authors read and approved the final manuscript.

References

- Koons GL, Diba M, Mikos AG. Materials design for bone-tissue engineering. *Nat Rev Mater*. 2020; 5(8): 584-603.
- Ghanbari E, Mehdipour A, Khazaei M, Khoshfeterat AB, Niknafs B. A review of recent advances on osteogenic applications of silk fibroin as a potential bio-scaffold in bone tissue engineering. *Int J Polym Mater Polym Biomater*. 2023; 31(1): 14-31.
- Noori A, Ashrafi SJ, Vaez-Ghaemi R, Hatamian-Zaremi A, Webster TJ. A review of fibrin and fibrin composites for bone tissue engineering. *Int J Nanomedicine*. 2017; 12: 4937-4961.
- Codreanu A, Balta C, Herman H, Cotoraci C, Mihali CV, Zurbau N, et al. Bacterial cellulose-modified polyhydroxyalkanoates scaffolds promotes bone formation in critical size calvarial defects in mice. *Materials (Basel)*. 2020; 13(6): 1433.
- Picheth GF, Pirich CL, Sierakowski MR, Woehl MA, Sakakibara CN, de Souza CF, et al. Bacterial cellulose in biomedical applications: a review. *Int J Biol Macromol*. 2017; 104(Pt A): 97-10.
- Huang C, Ye Q, Dong J, Li L, Wang M, Zhang Y, et al. Biofabrication of natural Au/bacterial cellulose hydrogel for bone tissue regeneration via in-situ fermentation. *Smart Mater Med*. 2023; 4: 1-4.
- Xiao J, Wei Q, Xue J, Liu Z, Li Z, Zhou Z, et al. Mesoporous bioactive glass/bacterial cellulose composite scaffolds for bone support materials. *Colloid Surf A*. 2022; 642: 128693.
- Abinaya S, Kavitha HP, Prakash M, Muthukrishnaraj A. Green synthesis of magnesium oxide nanoparticles and its applications: a review. *Sustain Chem Pharm*. 2021; 19: 1-9.
- Nasri-Nasrabadi B, Kaynak A, Heidarian P, Komeily-Nia Z, Mehra-sa M, Salehi H, et al. Sodium alginate/magnesium oxide nanocomposite scaffolds for bone tissue engineering. *Polym Adv Technol*. 2018; 29(34): 2553-2559.
- Suryavanshi A, Khanna K, Sindhu KR, Bellare J, Srivastava R. Magnesium oxide nanoparticle-loaded polycaprolactone composite electrospun fiber scaffolds for bone-soft tissue engineering applications: in-vitro and in-vivo evaluation. *Biomed Mater*. 2017; 12(5): 055011.
- Wang K, Ma Q, Zhang YM, Han GT, Qu CX, Wang SD. Preparation of bacterial cellulose/silk fibroin double-network hydrogel with high mechanical strength and biocompatibility for artificial cartilage. *Cellulose*. 2020; 27(4): 1845-1852.
- He Y, Ingudam S, Reed S, Gehring A, Strobaugh TP Jr, Irwin P. Study on the mechanism of antibacterial action of magnesium oxide nanoparticles against foodborne pathogens. *J Nanobiotechnology*. 2016; 14(1): 54.
- Naqvi QU, Kanwal A, Qaseem S, Naeem M, Ali SR, Shaffique M, et al. Size-dependent inhibition of bacterial growth by chemically engineered spherical ZnO nanoparticles. *J Biol Phys*. 2019; 45(2): 147-159.
- Hassan SE, Fouda A, Saied E, Farag MMS, Eid AM, Barghoth MG, et al. *Rhizopus oryzae*-mediated green synthesis of magnesium oxide nanoparticles (MgO-NPs): a promising tool for antimicrobial, mosquitocidal action, and tanning effluent treatment. *J Fungi (Basel)*. 2021; 7(5): 372.
- Nokoorani YD, Shamloo A, Bahadoran M, Moravvej H. Fabrication and characterization of scaffolds containing different amounts of allantoin for skin tissue engineering. *Sci Rep*. 2021; 11(1): 16164.
- Wang X, Liu M, Li H, Yin A, Xia C, Lou X, et al. MgO-incorporated porous nanofibrous scaffold promotes osteogenic differentiation of pre-osteoblasts. *Mater Lett*. 2021; 299: 130098.
- Rezakhani L, Alizadeh M, Sharifi E, Soleimannejad M, Alizadeh A. Isolation and characterization of crab haemolymph exosomes and its effects on breast cancer cells (4T1). *Cell J*. 2021; 23(6): 658-664.
- Khazaei F, Ghanbari E, Khazaei M. Protective effect of royal jelly against cyclophosphamide-induced thrombocytopenia and spleen and bone marrow damages in rats. *Cell J*. 2020; 22(3): 302-309.
- Hosseini FS, Soleimanifar F, Ardeshiryajimi A, Vakilian S, Mossahebi-Mohammadi M, Enderami SE, et al. In vitro osteogenic differentiation of stem cells with different sources on composite scaffold containing natural bioceramic and polycaprolactone. *Artif Cells Nanomed Biotechnol*. 2019; 47(1): 300-307.
- Pugazhendhi A, Prabhu R, Muruganantham K, Shanmuganathan R, Natarajan S. Anticancer, antimicrobial and photocatalytic activities of green synthesized magnesium oxide nanoparticles (MgONPs) using aqueous extract of *Sargassum wightii*. *J Photochem Photobiol B*. 2019; 190: 86-97.
- Ravoor J, Amirthalingam S, Mohan T, Rangasamy J. Antibacterial, anti-biofilm and angiogenic calcium sulfate-nano MgO composite bone void fillers for inhibiting *Staphylococcus aureus* infections. *Colloid Interface Sci Commun*. 2020; 39: 100332.
- Khan A, Shabir D, Ahmad P, Khandaker MU, Faruque M, Din IU. Biosynthesis and antibacterial activity of MgO-NPs produced from *Camellia-sinensis* leaves extract. *Mater Res Express*. 2020; 8(1): 015402.
- Hickey DJ, Ercan B, Sun L, Webster TJ. Adding MgO nanoparticles to hydroxyapatite-PLLA nanocomposites for improved bone tissue engineering applications. *Acta Biomater*. 2015; 14: 175-84.
- Xia X, Huang J, Wei J, Jin S, Zou Q, Zuo Y, et al. Magnesium oxide regulates the degradation behaviors and improves the osteogenesis of poly (lactide-co-glycolide) composite scaffolds. *Compos Sci Technol*. 2022; 222: 109368.
- Nokoorani YD, Shamloo A, Bahadoran M, Moravvej H. Fabrication and characterization of scaffolds containing different amounts of allantoin for skin tissue engineering. *Sci Rep*. 2021; 11(1): 16164.
- Suresh J, Pradheesh G, Alexramani V, Sundrarajan M, Hong SI. Green synthesis and characterization of hexagonal shaped MgO nanoparticles using insulin plant (*Costus pictus* D. Don) leave extract and its antimicrobial as well as anticancer activity. *Adv Powder Technol*. 2018; 29(7): 1685-1694.
- Numata Y, Mazzarino L, Borsali R. A slow-release system of bacterial cellulose gel and nanoparticles for hydrophobic active ingredients. *Int J Pharm*. 2015; 486(1-2): 217-225.
- Radwan-Pragłowska J, Janus Ł, Piątkowski M, Bogdał D, Matysek D. 3D hierarchical, nanostructured chitosan/PLA/HA scaffolds doped with TiO₂/Au/Pt NPs with tunable properties for guided bone tissue engineering. *Polymers (Basel)*. 2020; 12(4): 792.
- Khan MUA, Haider S, Haider A, Abd Razak SI, Kadir MRA, Shah SA, et al. Development of porous, antibacterial and biocompatible GO/n-HAp/bacterial cellulose/β-glucan biocomposite scaffold for bone tissue engineering. *Arab J Chem*. 2021; 14(2): 102924.
- Aydogdu MO, Ekren N, Suleymanoglu M, Erdem-Kuruca S, Lin CC, Bulbul E, et al. Novel electrospun polycaprolactone/graphene oxide/Fe₃O₄ nanocomposites for biomedical applications. *Colloids Surf B Biointerfaces*. 2018; 172: 718-727.
- Ghauri FA, Raza MA, Baig MS, Ibrahim S. Corrosion study of the graphene oxide and reduced graphene oxide-based epoxy coatings. *Mater Res Express*. 2017; 4(12): 125601.
- Ullah S, Zainol I, Idrus RH. Incorporation of zinc oxide nanoparticles into chitosan-collagen 3D porous scaffolds: Effect on morphology, mechanical properties and cytocompatibility of 3D porous scaffolds. *Int J Biol Macromol*. 2017; 104(Pt A): 1020-1029.
- Audtarat S, Hongsachart P, Dasri T, Chio-Srichan S, Soontaronon

- S, Wongsinlatam W, et al. Green synthesis of silver nanoparticles loaded into bacterial cellulose for antimicrobial application. *Nanocomposite*. 2022; 8(1): 34-46.
34. Khatami N, Khoshfetrat AB, Khaksar M, Zamani ARN, Rahbarghazi R. Collagen-alginate-nano-silica microspheres improved the osteogenic potential of human osteoblast-like MG-63 cells. *J Cell Biochem*. 2019; 120(9): 15069-15082.
35. De Silva RT, Mantilaka MMMGPG, Goh KL, Ratnayake SP, Amaratunga GAJ, de Silva KMN. Magnesium oxide nanoparticles reinforced electrospun alginate-based nanofibrous scaffolds with improved physical properties. *Int J Biomater*. 2017; 2017: 1391298.
36. Younis IY, El-Hawary SS, Eldahshan OA, Abdel-Aziz MM, Ali ZY. Green synthesis of magnesium nanoparticles mediated from *Rosa floribunda* charisma extract and its antioxidant, antiaging and anti-biofilm activities. *Sci Rep*. 2021; 11(1): 16868.
37. Xing X, Cheng G, Yin C, Cheng X, Cheng Y, Ni Y, et al. Magnesium-containing silk fibroin/polycaprolactone electrospun nanofibrous scaffolds for accelerating bone regeneration. *Arab J Chem*. 2020; 13: 5526-5538.
38. Domazetovic V, Marcucci G, Iantomasi T, Brandi ML, Vincenzini MT. Oxidative stress in bone remodeling: role of antioxidants. *Clin Cases Miner Bone Metab*. 2017; 14(2): 209-216.
39. Anastasio AT, Paniagua A, Diamond C, Ferlauto HR, Fernandez-Moure JS. Nanomaterial Nitric oxide delivery in traumatic orthopedic regenerative medicine. *Front Bioeng Biotechnol*. 2021; 8: 592008.
-